Title
Pathological crystal imaging with single-shot computational polarized light microscopy

Journal
Journal of Biophotonics, 13(1)

ISSN
1864-063X

Authors
Bai, Bijie
Wang, Hongda
Liu, Tairan
et al.

Publication Date
2020

DOI
10.1002/jbio.201960036

Peer reviewed

HHS Public Access

Author manuscript

J Biophotonics. Author manuscript; available in PMC 2021 May 06.

Published in final edited form as:

J Biophotonics. 2020 January ; 13(1): e201960036. doi:10.1002/jbio.201960036.

Pathological crystal imaging with single-shot computational polarized light microscopy

Bijie Bai[#1,2,3], **Hongda Wang**[#1,2,3], **Tairan Liu**[1,2,3], **Yair Rivenson**[1,2,3], **John FitzGerald**[4], **Aydogan Ozcan**[1,2,3,5,*]

[1]Electrical and Computer Engineering Department, University of California, Los Angeles, Los Angeles, California

[2]Bioengineering Department, University of California, Los Angeles, Los Angeles, California

[3]California NanoSystems Institute, University of California, Los Angeles, Los Angeles, California

[4]Division of Rheumatology, Department of Internal Medicine, David Geffen School of Medicine, University of California, Los Angeles, Los Angeles, California

[5]Department of Surgery, David Geffen School of Medicine, University of California, Los Angeles, Los Angeles, California

[#] These authors contributed equally to this work.

Abstract

Pathological crystal identification is routinely practiced in rheumatology for diagnosing arthritis disease such as gout, and relies on polarized light microscopy as the gold standard method used by medical professionals. Here, we present a single-shot computational polarized light microscopy method that reconstructs the transmittance, retardance and slow-axis orientation of a birefringent sample using a single image captured with a pixelated-polarizer camera. This method is fast, simple-to-operate and compatible with all the existing standard microscopes without extensive or costly modifications. We demonstrated the success of our method by imaging three different types of crystals found in synovial fluid and reconstructed the birefringence information of these samples using a single image, without being affected by the orientation of individual crystals within the sample field-of-view. We believe this technique will provide improved sensitivity, specificity and speed, all at low cost, for clinical diagnosis of crystals found in synovial fluid and other bodily fluids.

Graphical Abstract

[*]**Correspondence**: Aydogan Ozcan, University of California, Los Angeles, CA 90095. ozcan@ucla.edu.

CONFLICT OF INTEREST

A.O., B.B., and H.W. have a pending patent application on the presented technique. The remaining authors declare that they have no conflict of interest.

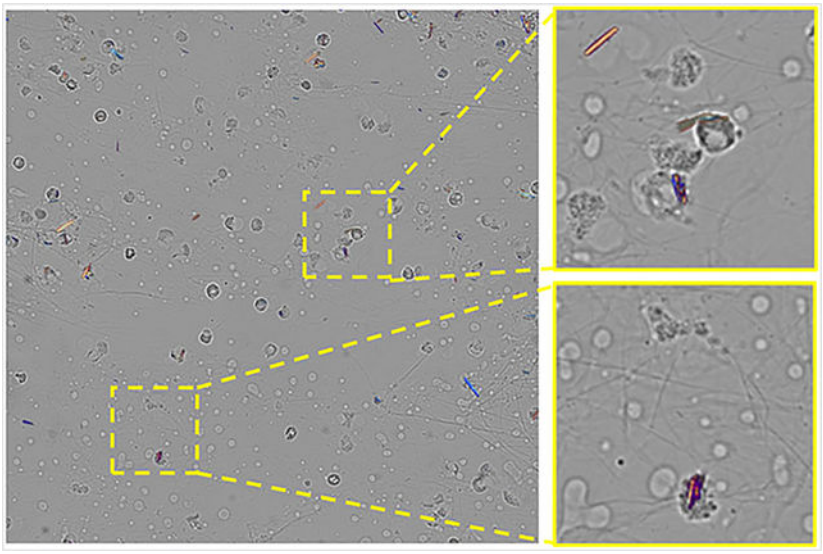

Keywords

arthritis; birefringence; computational imaging and microscopy; gout disease; pathological crystal; pixelated polarizer camera; rheumatology

1 | INTRODUCTION

Birefringence is an inherent characteristic of optically anisotropic materials that widely exist in human body, for example, collagen [1–4], amyloid [5–7], muscle [8, 9], skin [10, 11] as well as synovial fluid crystals [12, 13]. The pathological studies of such birefringent samples are often carried out with polarized light microscopy [14] and have shown clinical value in observing squamous cell carcinoma [1], articular cartilage [2, 3], cerebral amyloid [5], primary cutaneous amyloidosis [6], senile cardiovascular amyloid [7], monosodium urate (gout) and calcium pyrophosphate (pseudogout) crystals [15, 16]. For these applications, a widely practiced method is compensated polarized light microscopy (CPLM), which converts the birefringence of the object into color variations with a pair of linear polarizers and a full-wave retardation plate (i.e., the compensator) [17]; this method has been used as the gold standard for the diagnosis of gout and pseudogout [12, 13], caused by the deposition of monosodium urate (MSU) crystals and calcium pyrophosphate dihydrate (CPPD) crystals in the joints, respectively [15, 16]. Under a CPLM, the orientation of the optical axis of each crystal is indicated by yellow or blue colors, modulated by the angle between the optical axis and the full wave retardance plate. Although simple to operate, CPLM requires manual alignment of polarizers and rotation of the retardance plate to confirm low-contrast features, while only providing qualitative results. These factors limit the sensitivity of CPLM to detect smaller crystals and crystals with weak birefringence, giving poor contrast with respect to the background, typical of for example, CPPD crystals, [18] and are compounded by examiner experience [19].

Efforts have been made to create new approaches for quantitative polarized light microscopy [20–22]. To reconstruct the full Stokes parameters of polarized light, these approaches capture several images while mechanically or electronically rotating the polarizers, which unavoidably adds complexity and cost to the imaging system, and limits the imaging frame rate. As an alternative approach, one can encode the polarization information with pixel-based polarizers on the focal plane, which is often referred to as pixelated polarizer camera; in fact, this approach has been utilized for various applications, in for example, metrology, polarimetry, interferometry and microscopy [23–27].

Here, we demonstrate a single-shot computational polarized light microscopy (SCPLM) method using a polarization image sensor that can be used to identify pathological crystals in synovial fluid and other bodily fluids. Compared with the gold standard method (CPLM) frequently used in rheumatology, the presented approach is faster, provides better contrast regardless of the orientation or size of the individual crystals, and requires minimum modification of a standard light microscope. By providing quantitative retardance and orientation map of the sample, our method can generate pseudo-colored images from a single frame, closely resembling the color information of traditional CPLM images with a major improvement in contrast, which can significantly benefit physicians in clinical diagnosis. To demonstrate the success of this approach, we imaged MSU and CPPD crystals found in deidentified synovial fluid aspirates from patients, as well as triamcinolone acetonide (TCA) crystals, which can be confused with CPPD in synovial fluid [28]. Our results confirm the strong potential of this computational polarized light microscopy technique as a valuable instrument for the detection and inspection of pathological crystals in bodily fluids.

2 | MATERIALS AND METHODS

2.1 | Experimental setup

Our SCPLM method is demonstrated with a conventional bright-field microscope (IX83, Olympus), as shown in Figure 1A. The incoherent illumination is provided by a light emitting diode (LED, Part# M455L3-C1, Thorlabs) at 455 nm with a bandwidth of 18 nm. A left-hand circular polarizer (SKU# 88–086, Edmund Optics) is mounted on a 3D-printed holder and placed between the light source and the birefringent sample. The samples are imaged using a ×20/0.75NA objective lens (UPLSAPO 20X, Olympus) with a ×2 magnification changer (Model# IX3-CAS, Olympus) and captured with a polarization complementary metal-oxide-semiconductor (CMOS) image sensor (PHX050S-PC, LUCID Vision Labs) which has 2448 × 2048 pixels, each with a size of 3.45 μm. The sensor utilizes four different directional polarizing filters (0°, 90°, 45°, and 135°) that form a repeating pattern across the CMOS image sensor, so that each one of them is able to measure the polarization component along a specific orientation. An SEM picture [29] of these four different types of polarizing filters on the CMOS sensor is shown in the inset of Figure 1A.

As illustrated in Figure 1B, LED illumination light passes through a left-hand circular polarizer and is transmitted through a birefringent sample. The transmitted light is modulated to become elliptically polarized, where the polarization status is dependent on the orientation and the birefringence of the sample. Finally, the image of the sample with the

corresponding polarization information is focused on the pixelated polarizer CMOS sensor and digitally captured for further analysis.

The CPLM images (used for comparison purposes) are captured using an Olympus BX51 microscope with additional polarization components, a drop-in polarizer (Model# U-POT, Olympus) and a gout analyzer (Model# U-GAN, Olympus), using a ×40/0.75NA objective lens (UPLFLN 40X, Olympus) and a color charge-coupled device (CCD) image sensor (Retiga-2000R, QImaging).

We imaged MSU, CPPD and TCA crystals to demonstrate the performance of our SCPLM method. MSU and CPPD crystal samples were obtained from existing and discarded specimen, deidentified synovial fluid aspirates from patients with joint effusions. TCA crystals were obtained from Bristol-Myers Squibb TCA injectable suspension (40 mg/mL).

2.2 | Birefringence calculations

We formulated the polarization imaging capability of our system using the Jones calculus [30, 31], in which the polarization status of light is represented by a Jones vector and the linear optical elements are represented by Jones matrices. The light field that is transmitted through an object can be written as:

$$E_{\text{out}} = M_{\text{detector}}\, M_{\text{object}}\, M_{\text{polarizer}} \cdot E_{\text{in}} \tag{1}$$

where E_{in} represents the incident light, M_{detector}, M_{object} and $M_{\text{polarizer}}$ represent the Jones matrices of the directional polarizing filters on the image sensor pixels, the birefringent sample of interest, and the circular polarizer, respectively. For a pixel on the CMOS image sensor with 0°-polarization filter, the resulting electric field can be formulated as:

$$E^0_{\text{out}} = \begin{pmatrix} 1 & 0 \\ 0 & 0 \end{pmatrix} \cdot \begin{pmatrix} \cos\frac{\Delta}{2} + i\sin\frac{\Delta}{2}\cos 2\phi & i\sin\frac{\Delta}{2}\sin 2\phi \\ i\sin\frac{\Delta}{2}\sin 2\phi & \cos\frac{\Delta}{2} - i\sin\frac{\Delta}{2}\cos 2\phi \end{pmatrix} \cdot \frac{1}{2}\begin{pmatrix} 1 & -i \\ i & 1 \end{pmatrix} \cdot E_{\text{in}} \tag{2}$$

where Jones matrix M_{object} represents the polarization property of any arbitrary birefringent object with a retardance magnitude of Δ and a slow axis orientation of ϕ [31]. The retardance is given by $\Delta = \frac{2\pi}{\lambda}\Delta n \cdot t$, where Δn refers to the refractive index difference between the slow and fast axes of the sample, calculated at the illumination wavelength λ, and t is the thickness of the sample. Note that both Δ and ϕ are spatially variant and therefore can be denoted by $\Delta(x, y)$ and $\phi(x, y)$. The intensity value captured by this 0°-orientated pixel can be expressed as:

$$I_0 \propto \left|E^0_{\text{out}}\right|^2 = E^0_{\text{out}} \cdot E^0_{\text{out}\,*} \tag{3}$$

where $E^0_{\text{out}\,*}$ represents the complex conjugate of E^0_{out}. Inserting Equation (2) into Equation (3), we get:

$$I_0 = \frac{1}{4} I_{\max}(1 - \sin\Delta\sin 2\phi) \tag{4}$$

where $I_{\max}$ is the intensity of the illumination light. Similarly, the intensity values captured by pixels along the other three directions can be expressed as:

$$\begin{aligned} I_{45} &= \frac{1}{4} I_{\max}(1 + \sin\Delta\cos 2\phi), \\ I_{90} &= \frac{1}{4} I_{\max}(1 + \sin\Delta\sin 2\phi), \\ I_{135} &= \frac{1}{4} I_{\max}(1 - \sin\Delta\cos 2\phi) \end{aligned} \tag{5}$$

Combining all the four equations in Equations (4) and (5), we can introduce the following two auxiliary variables:

$$\begin{aligned} A &= \frac{I_{90} - I_0}{I_{90} + I_0} = \sin\Delta\sin 2\phi \\ B &= \frac{I_{45} - I_{135}}{I_{45} + I_{135}} = \sin\Delta\cos 2\phi \end{aligned} \tag{6}$$

Finally, the retardance magnitude and the slow axis orientation of the birefringent object can be reconstructed using Equation (6) as:

$$\begin{aligned} \Delta &= \arcsin\sqrt{A^2 + B^2} \\ \phi &= \frac{1}{2}\arctan\frac{A}{B} \end{aligned} \tag{7}$$

2.3 | Pseudo-coloring

Once the retardance and the slow-axis orientation of the sample are reconstructed using a single frame captured with our SCPLM, we can apply pseudo-coloring to better visualize the image of the sample. For this purpose, we represented the retardance value with the image intensity (Figure 2C), encoded the slow axis orientation with a rainbow colormap that is crafted to closely resemble the traditional CPLM image (Figure 2D), and combined these two channels into a pseudo-colored SCLPM image (Figure 2E). We also visualized both the birefringent and nonbirefringent components in the sample field of view by digitally overlaying the pseudo-colored SCPLM image with the bright-field transmittance image of the same field of view, which is simply obtained from the same input image by averaging the four polarization channels, see Figure 2F for an example of this digitally fused SCPLM image.

3 | RESULTS AND DISCUSSION

We demonstrated the success of our method by imaging MSU, CPPD and TCA crystals, and compared the reconstructed pseudo-colored SCPLM images with the corresponding images acquired using a traditional CPLM with the compensator at orthogonal settings, as shown in

Figure 3. Some of the crystals with weak birefringence in the sample field of view are not easily visible and further hindered by their random orientation with respect to the fixed angles of the compensator in the CPLM images. Figure 3A–D,E–H demonstrate images of MSU and CPPD crystals found in the synovial fluid of patients with gout and pseudogout, respectively. Figure 3I–L further show images of TCA crystals that can be confused with CPPD in synovial fluid samples. The liquid drying artifacts that might sometimes appear during the sample preparation process (Figure 3M–P) and some of the background cells in the sample fluid (Figure 3Q–T) can also show weak birefringence. In these cases, the SCPLM generated images (Figure 3N,R) help us differentiate crystals from other microscopic features and objects within the sample. Since some of these crystals are within a fluidic sample, they may unavoidably flow around and change their relative positions between CPLM and SCPLM experiments, as highlighted in Figure 3I–L. As can be seen in this comparison, SCLPM performs very well for all these tested crystal samples, rejects nonbirefringent background signals and reveals the crystals with significantly better contrast using a single image acquisition. Therefore, SCPLM is especially beneficial for screening small birefringent objects within a noisy background, for example when crystals are intracellular (Figure 3Q–T). As an example, we imaged synovial fluid samples taken from gout patients during a clinical attack where MSU crystals have been phagocytosed into white blood cells, as shown in Figure 4. The digitally fused SCPLM images clearly highlight the MSU crystals and its surrounding inflammatory debris.

This single-shot operation of our method also eliminates the need for rotating the polarizer and/or the compensator in CPLM and improves the imaging speed on the same optical setup. The computational reconstruction algorithm implemented in MATLAB takes ~2 s to reconstruct a 1 mm^2 field-of-view (with ~134 megapixels in the raw image) using a consumer-grade desktop computer equipped with Intel i9–7900X central processing unit (CPU). The reconstruction time can be further shortened by for example, >10 fold with C/C ++ programming and the use of graphics processing units (GPU) [32]. Unlike the traditional CPLM images that are dependent on the orientation of the polarizer, the birefringence measurements using SCPLM are independent of the crystal orientation (Figure 5), and therefore SCPLM is ready to be integrated into existing clinical workflow with minimum modification of existing imaging hardware.

To highlight the advantages of SCPLM images, in this work we used synovial fluid samples that are rich with crystal deposition (Figures 3–5). In clinical practice, dozens of ×4 or ×10 low to medium power fields might need to be searched to find scant or small crystals. The stronger contrast of SCPLM images would make searching for these crystals much more efficient and more sensitive. The quantitative polarization information created by SCPLM also provides more insights into the sample and will potentially benefit the development of machine learning-based automated processing and diagnostic analysis of pathological crystal samples.

4 | CONCLUSIONS

We introduced a computational single-shot polarizing light microscopy method, termed SCPLM, which achieves quantitative polarization imaging of samples. We demonstrated our

method by imaging MSU, CPPD and TCA crystals and reconstructed their birefringence images. The reconstructed images were pseudo-colored to resemble CPLM images, the clinical gold standard used for identification of MSU and CPPD crystals. We believe this new method will broadly benefit the field of pathological crystal studies and potentially create new quantitative standards for clinical diagnosis in rheumatology.

ACKNOWLEDGMENT

The authors acknowledge the support of National Institutes of Health (R21AR072946).

REFERENCES

[1]. Arun Gopinathan P, Kokila G, Jyothi M, Ananjan C, Pradeep L, Humaira Nazir S, Scientifica (Cairo) 2015, 2015, 802980. [PubMed: 26587310]

[2]. Király K, Hyttinen MM, Lapveteläinen T, Elo M, Kiviranta I, Dobai J, Módis L, Helminen HJ, Arokoski JP, Histochem. J 1997, 29, 317. [PubMed: 9184847]

[3]. Changoor A, Tran-Khanh N, Méthot S, Garon M, Hurtig MB, Shive MS, Buschmann MD, Osteoarthr. Cartil 2011, 19, 126.

[4]. Orberg J, Baer E, Hiltner A, Connect. Tissue Res 1983, 11, 285. [PubMed: 6227451]

[5]. Jin L-W, Claborn KA, Kurimoto M, Geday MA, Maezawa I, Sohraby F, Estrada M, Kaminksy W, Kahr B, Proc. Natl. Acad. Sci. USA 2003, 100, 15294. [PubMed: 14668440]

[6]. Vijaya B, Dalal BS, Sunila, and Manjunath GV, Indian J. Pathol. Microbiol 55, 170–174 (2012). [PubMed: 22771637]

[7]. Cornwell GG, Murdoch WL, Kyle RA, Westermark P, Pitkänen P, Am. J. Med 1983, 75, 618. [PubMed: 6624768]

[8]. Schapira G, Dreyfus J-C, Joly M, Nature 1952, 170, 494.

[9]. Adams DC, Hariri LP, Miller AJ, Wang Y, Cho JL, Villiger M, Holz JA, Szabari MV, Hamilos DL, Scott Harris R, Griffith JW, Bouma BE, Luster AD, Medoff BD, Suter MJ, Sci. Transl. Med 2016, 8, 359ra131.

[10]. Pierce MC, Strasswimmer J, Park H, Cense B, de Boer JF, J. Biomed. Opt 2004, 9, 287. [PubMed: 15065893]

[11]. Jacques SL, Ramella-Roman JC, Lee K, J. Biomed. Opt 2002, 7, 329. [PubMed: 12175282]

[12]. Mccarty DJ, Hollander JL, Ann. Intern. Med 1961, 54, 452. [PubMed: 13773775]

[13]. Pascual E, Batlle-Gualda E, Martínez A, Rosas J, Vela P, Ann. Intern. Med 1999, 131, 756. [PubMed: 10577299]

[14]. Wolman M, J. Histochem. Cytochem 1975, 23, 21. [PubMed: 1090645]

[15]. Mccarty DJ, Kohn NN, Faires JS, Ann. Intern. Med 1962, 56, 711.

[16]. McGill NW, Dieppe PA, Ann. Rheum. Dis 1991, 50, 558. [PubMed: 1888197]

[17]. Gatter RA, Arthritis Rheum. 1974, 17, 253. [PubMed: 4363486]

[18]. Rosenthal A, Ryan L, McCarty D, Arthritis and Allied Conditions: A Textbook of Rheumatology, 14th ed., Lippincott Williams & Wilkins, Philadelphia, PA 2001, p. 2348.

[19]. Park JW, Ko DJ, Yoo JJ, Chang SH, Cho HJ, Kang EH, Park JK, Song YW, Lee YJ, Korean J Intern. Med 2014, 29, 361.

[20]. Oldenbourg R, Mei G, J. Microsc 1995, 180, 140. [PubMed: 8537959]

[21]. Goldman RD, Spector DL, Live Cell Imaging: A Laboratory Manual, Cold Spring Harbor Laboratory Press, Cold Spring Harbor, NY 2005, p. 205.

[22]. Zhang Y, Lee SYC, Zhang Y, Furst D, Fitzgerald J, Ozcan A, Sci. Rep 2016, 6, 28793. [PubMed: 27356625]

[23]. Chun CSL, Fleming DL, Torok EJ, Polarization-sensitive thermal imaging, in Automatic Object Recognition IV (International Society for Optics and Photonics), Orlando, FL 1994, Vol. 2234, pp. 275–286.

[24]. Nordin GP, Meier JT, Deguzman PC, Jones MW, J. Opt. Soc. Am. A 1999, 16, 1168.

[25]. Brock N, Kimbrough BT, Millerd JE, A pixelated micropolarizer-based camera for instantaneous interferometric measurements, in Polarization Science and Remote Sensing V (International Society for Optics and Photonics), San Diego, CA 2011, Vol. 8160, p. 81600W.

[26]. Tyo JS, Goldstein DL, Chenault DB, Shaw JA, Appl. Optics, AO 2006, 45, 5453.

[27]. Tian X, Tu X, Croce KD, Yao G, Cai H, Brock N, Pau S, Liang R, Biomed. Opt. Express, BOE 2019, 10, 1638. [PubMed: 31061760]

[28]. Kahn CB, Hollander JL, Schumacher HR, JAMA 1970, 211, 807. [PubMed: 4320615]

[29]. Yamazaki T, Maruyama Y, Uesaka Y, Nakamura M, Matoba Y, Terada T, Komori K, Ohba Y, Arakawa S, Hirasawa Y, Kondo Y, Murayama J, Akiyama K, Oike Y, Sato S, Ezaki T, Four-directional pixel-wise polarization CMOS image sensor using air-gap wire grid on 2.5-μm back-illuminated pixels, in 2016 IEEE International Electron Devices Meeting (IEDM) San Francisco, CA 2016, pp. 8.7.1–8.7.4.

[30]. Hurwitz H, Jones RC, J. Opt. Soc. Am 1941, 31, 493.

[31]. Shribak M, Oldenbourg R, Appl. Optics 2003, 42, 3009.

[32]. Isikman SO, Bishara W, Mavandadi S, Yu FW, Feng S, Lau R, Ozcan A, Proc. Natl. Acad. Sci. USA 2011, 108, 7296. [PubMed: 21504943]

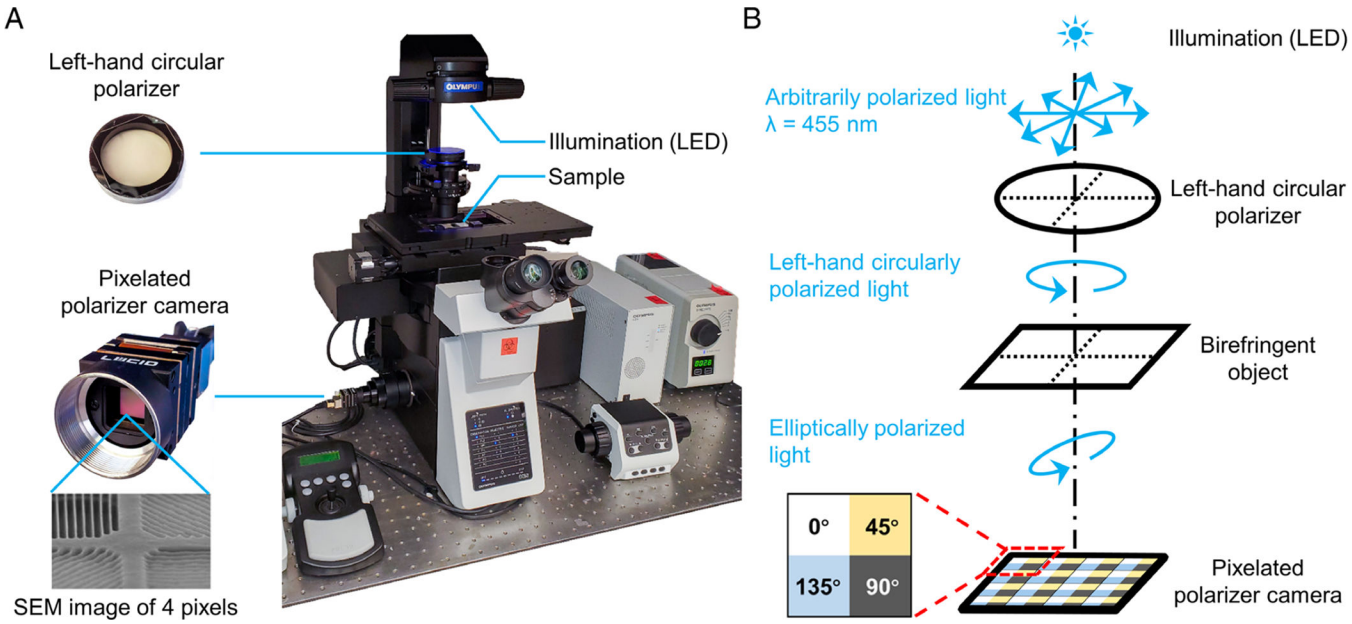

FIGURE 1.

A, Single-shot computational polarized light microscopy (SCPLM) setup. B, Schematic diagram of the SCPLM setup. SEM image is adapted from Reference [29] with permission

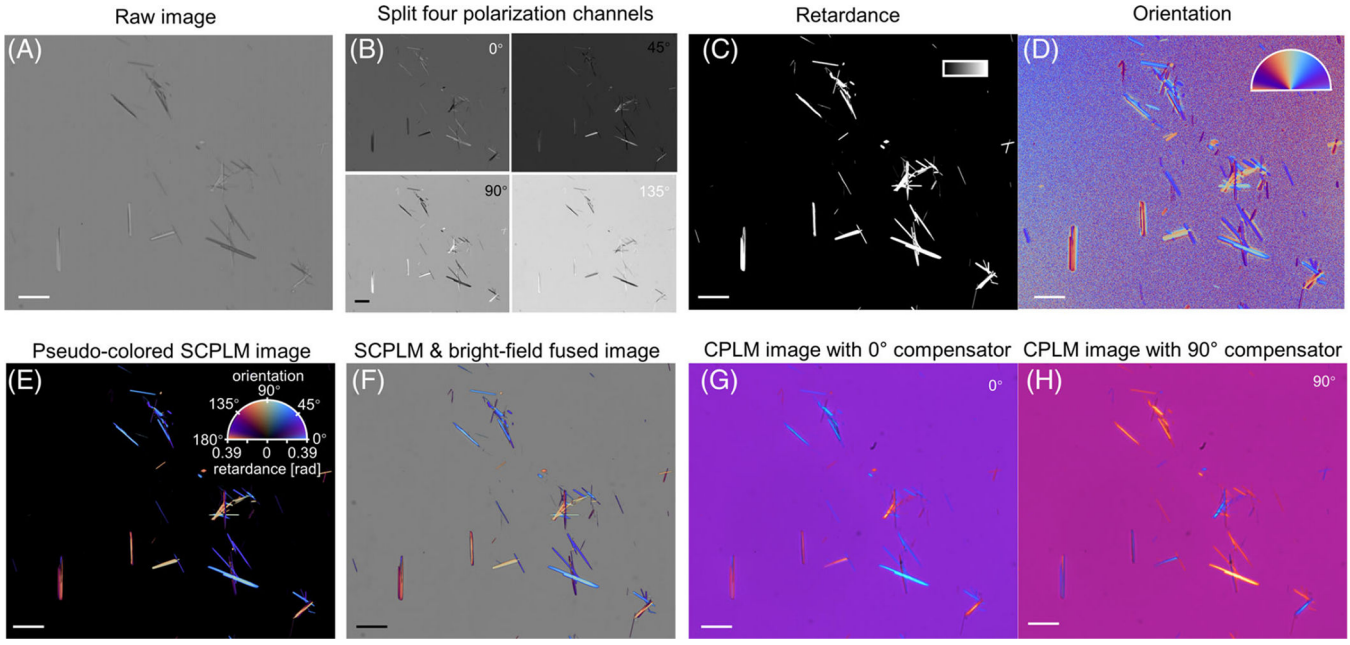

FIGURE 2.

Schematic diagram of the birefringence measurement and pseudo-coloring. A, Raw image captured with our SCPLM. B, Intensity images extracted from the four polarization channels of the image shown in (A). C, D, Reconstructed retardance and orientation maps of the sample, calculated from (B). Colormap in (C): 0–0.39 rad. Colormap in (D): 0–180°. E, Pseudo-colored SCPLM image. F, Overlay of the pseudo-colored SCPLM image with the bright-field transmittance image, calculated by averaging the four polarization channels of the same image. Both of the images shown in (E) and (F) only use the information acquired in (A). G, H, CPLM images of the same sample with the compensator at 0° and 90°, respectively. Scale bar in all figures represents 20 μm

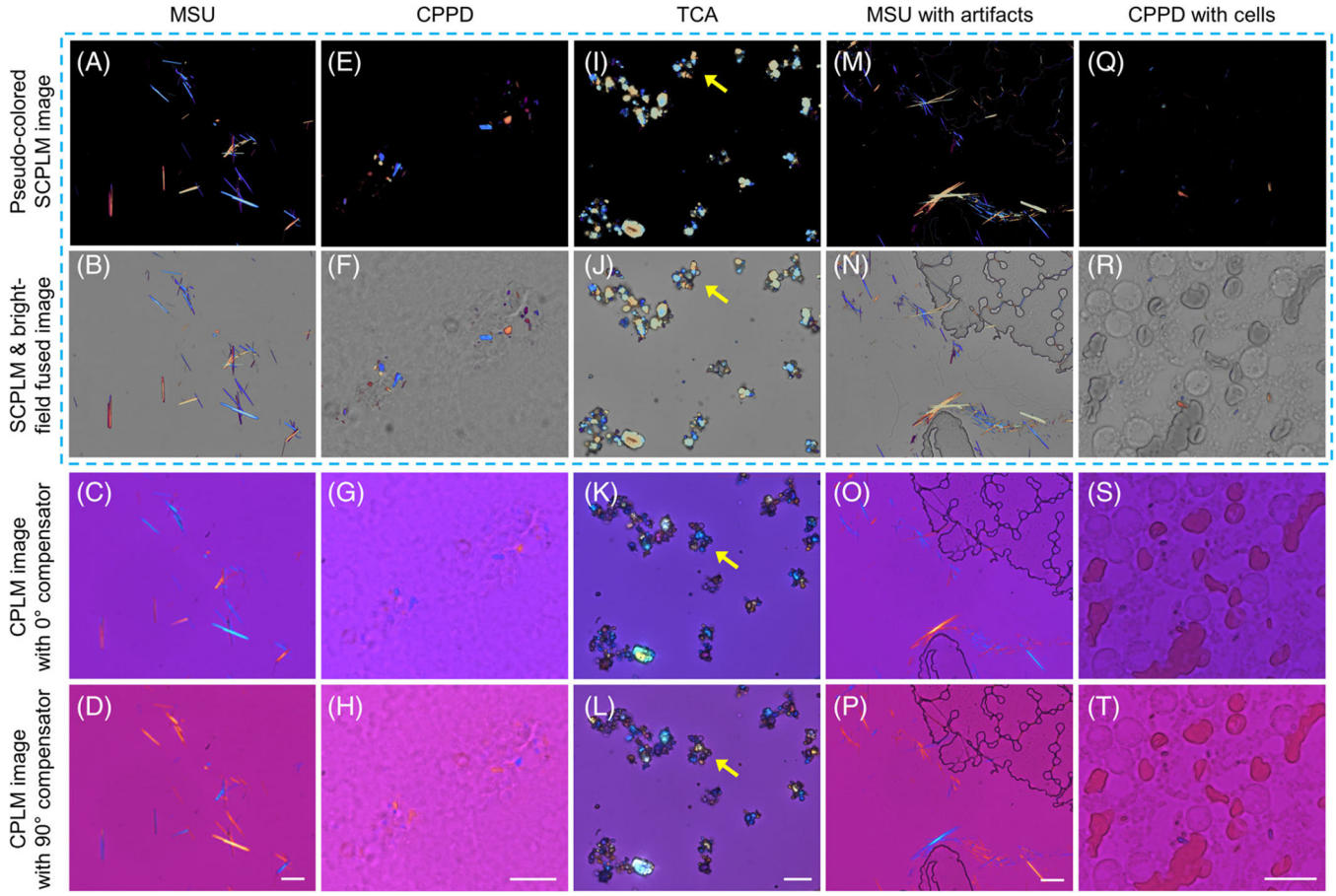

FIGURE 3.

Experimentally captured SCPLM and CPLM images of (A-D) MSU, (E-H) CPPD, (I-L) TCA, (M-P) MSU with sample preparation artifacts in the background, and (Q-T) CPPD crystals distributed among cells. All the SCPLM images are calculated from a single raw image of the corresponding field of view, and are pseudo-colored with the same colormap of the slow-axis orientation. Scale bar in all figures represents 20 μm

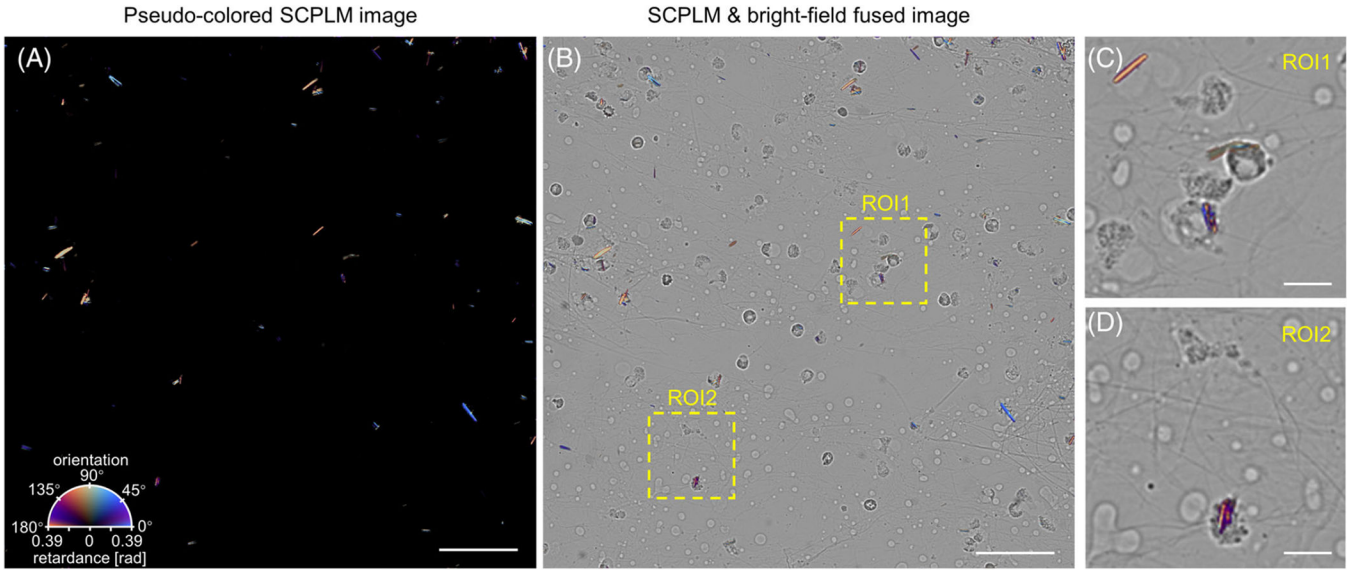

FIGURE 4.

Experimentally captured SCPLM images showing MSU crystals engulfed by white blood cells. A, Pseudo-colored SCPLM image. B, Overlay of the pseudo-colored SCPLM image with the bright-field transmittance image. C, D, Two regions of interest (ROIs) showing the digitally fused SCPLM images with MSU in the white blood cells. Scale bar in (A, B) represents 50 μm and scale bar in (C, D) represents 10 μm

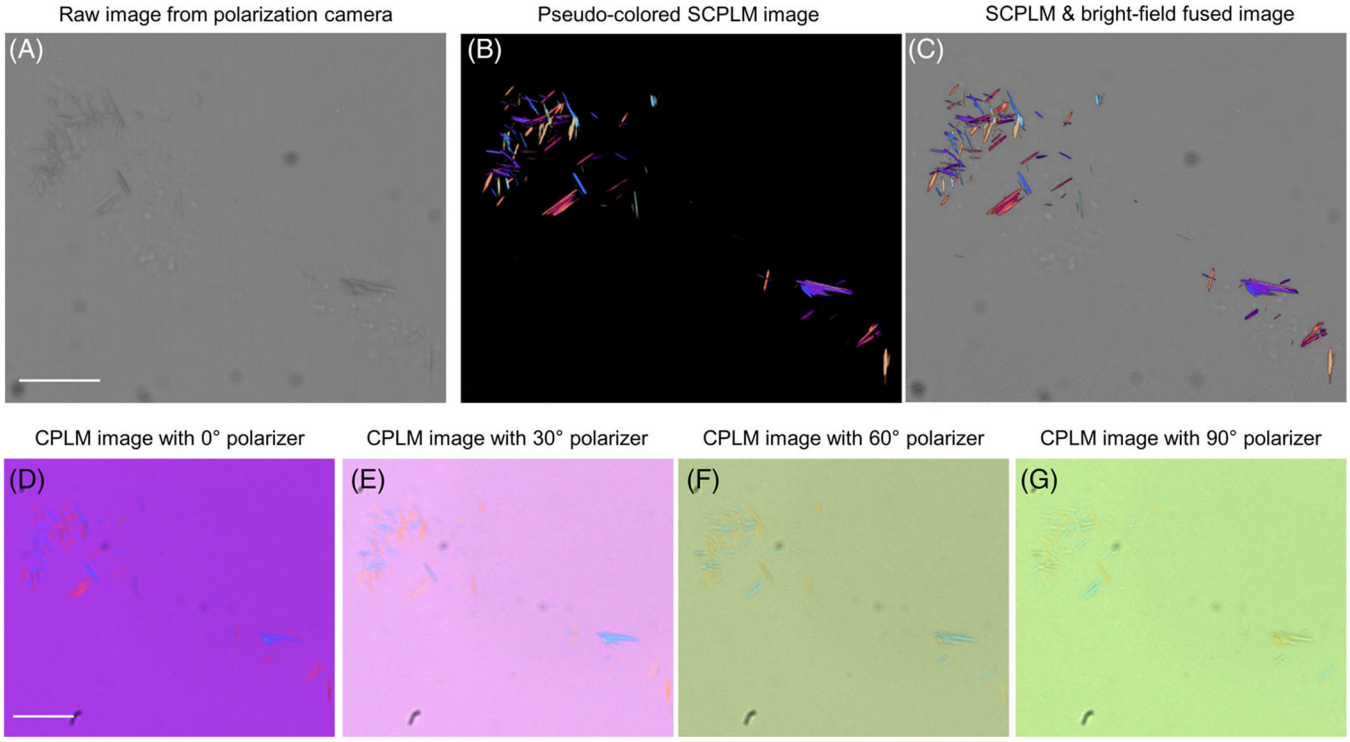

FIGURE 5.

(A-C) SCPLM image quality is independent of the orientation of the sample or the polarizer. (D-G) Traditional CPLM images require the alignment of the orientations of the polarizer, the sample and the compensator. These subfigures illustrate that when the polarizer rotates, CPLM image contrast significantly varies. Scale bar in all figures represents 20 μm